J Solid State Electrochem (2006) 10: 28–40
DOI 10.1007/s10008-005-0650-1

ORIGINAL PAPER

A. L. Shaula · V. V. Kharton · F. M. B. Marques
A. V. Kovalevsky · A. P. Viskup · E. N. Naumovich

# Oxygen permeability of mixed-conducting composite membranes: effects of phase interaction

Received: 6 December 2004 / Revised: 20 December 2004 / Accepted: 4 January 2005 / Published online: 6 April 2005


**Abstract** Composite ceramic membranes, based on selected combinations of ionic conductors ($(La_{0.9}Sr_{0.1})_{0.98}Ga_{0.8}Mg_{0.2}O_{3-\delta}$—LSGM or $Ce_{0.8}Gd_{0.2}O_{2-\delta}$—CGO) and electronic/mixed conductors ($La_2Ni_{0.8}Cu_{0.2}O_{4+\delta}$—LNC, $La_{0.8}Sr_{0.2}Fe_{0.8}Co_{0.2}O_{3-\delta}$—LSFC, $La_{0.7}Sr_{0.3}MnO_{3-\delta}$—LSM, and $SrCoO_{3-\delta}$ – $Sr_2Fe_3O_{6.5\pm\delta}$—SCSF), were processed and characterized aiming at the identification of key features to be considered in the design and optimization of materials performance as mixed conductors. Although after almost complete reaction between constituents, the best permeability was observed for the LSGM/LSFC combination processed under moderate firing conditions. Ceria-based composites, while preserving a typical composite microstructure, and suffering small compositional changes due to interaction between constituents, behaved always below the result of an ideal combination of the best characteristics of the individual components. Materials interaction, from modest compositional changes to formation of new phases, with deep changes in nominal composition, can be understood both as a challenge requiring proper identification of ideal processing conditions for phase preservation, but also as an opportunity for the development of entirely new composites and materials with compositional heterogeneities at grain size level.

A. L. Shaula · V. V. Kharton · F. M. B. Marques
A. V. Kovalevsky · E. N. Naumovich
Department of Ceramics and Glass Engineering,
CICECO, University of Aveiro,
3810-193 Aveiro, Portugal

V. V. Kharton (✉) · A. V. Kovalevsky · A. P. Viskup
E. N. Naumovich
*Present address*: Institute of Physicochemical Problems,
Belarus State University, 14 Leningradskaya Str,
220050 Minsk, Belarus
E-mail: kharton@cv.ua.pt
Tel.: +351-234-370263
Fax: +351-234-425300

**Keywords** Mixed conductor · Oxygen permeation · Oxide composite · Ionic conductivity · Phase interaction

## Introduction

Solid oxides with mixed oxygen ionic and electronic conductivity are of great interest due to their potential applications in high-temperature gas separation and catalytic reactions such as partial oxidation of hydrocarbons and other electrochemical devices [1–3]. The use of dense mixed-conductive ceramic membranes may provide significant economical benefits for commercial Fischer–Tropsh synthesis of hydrocarbons, combining air separation, steam reforming and partial oxidation in one single reactor, and decreasing considerably the cost of synthesis gas production [4, 5]. Perovskite-related phases $(A,Ln)(Co,Fe)O_{3-\delta}$ (A = Sr, Ba; Ln is the rare-earth element) have been widely studied due to their high electronic and significant oxygen ionic conductivities. Generally, perovskite-based materials, that exhibit high oxygen permeation fluxes, demonstrate thermodynamic and/or dimensional instability under large oxygen chemical potential gradients such as "air/methane" and may react with gaseous species, such as $CO_2$, showing decreasing oxygen permeability with time [6, 7]. This shows how problematic is matching the characteristics of single-phase solid oxide with all industrial requirements.

In multi-phase ceramics certain properties may be provided by different phases. As a result, composites can benefit from each component contribution to achieve the necessary performance. Therefore, various materials combinations were tested and the corresponding composites were examined [8–19]. The typical dual-phase systems obtained included one phase showing high electronic transport and the other phase being a fast ionic conductor. The conductivity of a composite depends strongly on components volume

ratio. To prepare high oxygen-permeable solid oxides, both phases should form a continuous network so that oxygen transport through the ionic conductive phase is balanced by the electronic current through the electronic conductive phase. Percolation in a composite requires the minor component content to be usually higher than 30 vol%. Total conductivity and oxygen permeability measurements in systems like noble elements (Ag, Au and Pd) combined with a solid electrolyte such as yttria-stabilized zirconia (YSZ), $Bi_{1.5}Er_{0.5}O_3$ and $Bi_{1.5}Y_{0.3}Sm_{0.2}O_3$ were found promising [9, 10, 14]. However, these ceramic–metal membranes are expensive for practical applications, and solid oxides with dominant electronic transport have been used to replace noble metals [8, 12, 13, 15, 17–19]. In the latter case, however, materials and processing conditions should be selected taking into account reactivity, as cation interdiffusion leads very often to additional phase formation and/or the composite performance is lower than that of the precursor materials [8, 12, 17, 18].

In order to identify trends in the development of oxide composite ceramics, the present work will summarize and compare experimental data on model systems, including $(La_{0.9}Sr_{0.1})_{0.98}Ga_{0.8}Mg_{0.2}O_{3-\delta}$ – $La_{0.8}Sr_{0.2}Fe_{0.8}Co_{0.2}O_{3-\delta}$ (LSGM/LSFC), $(La_{0.9}Sr_{0.1})_{0.98}Ga_{0.8}Mg_{0.2}O_{3-\delta}$ – $La_2Ni_{0.8}Cu_{0.2}O_{4+\delta}$ (LSGM/LNC), $Ce_{0.8}Gd_{0.2}O_{2-\delta}$ – $La_{0.8}Sr_{0.2}Fe_{0.8}Co_{0.2}O_{3-\delta}$ (CGO/LSFC), $Ce_{0.8}Gd_{0.2}O_{2-\delta}$ – $La_{0.7}Sr_{0.3}MnO_{3-\delta}$ (CGO/LSM), and $SrCoO_{3-\delta}$ – $Sr_2Fe_3O_{6.5\pm\delta}$ (SCSF) composites. For almost pure ionic conductivity, CGO and LSGM seem most favorable due to their large oxygen pressure range of stability when compared to the $\delta$-phase $Bi_2O_3$-based ceramics, and higher ionic conductivity if compared to YSZ , e.g. [1]. To achieve the required electronic conductivity, perovskite-related $La_2Ni_{0.8}Cu_{0.2}O_{4\pm\delta}$, $La_{0.7}Sr_{0.3}MnO_{3-\delta}$ and $La_{0.8}Sr_{0.2}Fe_{0.8}Co_{0.2}O_{3-\delta}$, all having acceptable thermal expansion [13, 19, 20], were used in combination with these solid electrolytes. The SCSF composites are based on perovskite-type $Sr(Co,Fe)O_{3-\delta}$, exhibiting one of the highest levels of oxygen permeability [21], but possessing excessively high thermal and chemical induced expansion, resulting in membrane degradation [22]. On the contrary, relatively high stability and a substantial ionic transport combined with low TECs were reported for orthorhombic $Sr_2(Fe,Co)_3O_{6.5\pm\delta}$ [23]. Recent work also shows quite complex equilibria in the $Sr_2(Fe,Co)_3O_{6.5\pm\delta}$ system, with a phase composition strongly dependent on temperature and oxygen pressure [24, 25]. On heating in air, $Sr_2(Fe,Co)_3O_{6.5\pm\delta}$ decomposes into a two- or three-phase mixture comprising $Sr(Co,Fe)O_{3-\delta}$ and $Co(Fe)O_{1+\delta}$; the oxygen permeability of multiphase ceramics is determined by the content of the perovskite phase, whilst the ionic transport in $Sr_2Fe_3O_{6.5}$-based solid solution is rather low [25]. As $Fe_{1-x}Co_xO_y$ is rather insulating, attention was drawn to dual-phase composites consisting of $Sr_2(Fe,Co)_3O_{6.5\pm\delta}$ and $Sr(Fe,Co)O_{3-\delta}$ solid solutions.

## Experimental

Commercially available powders of $Ce_{0.8}Gd_{0.2}O_{2-\delta}$ (CGO), $La_{0.8}Sr_{0.2}Fe_{0.8}Co_{0.2}O_{3-\delta}$ (LSFC), $La_{0.7}Sr_{0.3}MnO_{3-\delta}$ (LSM) and $(La_{0.9}Sr_{0.1})_{0.98}Ga_{0.8}Mg_{0.2}O_{3-\delta}$ (LSGM), produced by Praxair Specialty Ceramics (Seattle), were used for the preparation of CGO/LSFC, CGO/LSM and LSGM/LSFC composites. To prepare CGO/LSFC and CGO/LSM mixtures, the powders of CGO, LSFC and LSM were annealed in air at 1370 K for 6 h, slowly cooled and homogenized by ball-milling during 7–10 h. Preliminary studies of the LSGM/LSFC system suggested a need for passivation of LSGM and/or LSFC grains [26]. Therefore, the LSGM powder was coarsened by thermal treatment in air at 1423 K mol °C during 4 h and then mixed with LSFC powder in an agate mortar. The ceramic samples were fabricated in different sintering conditions in order to study the influence of the interaction between initial components on the characteristics of produced materials.

The powder of $La_2Ni_{0.8}Cu_{0.2}O_{4+\delta}$ (LNC) with submicron particle size was synthesized via the glycine-nitrate process (GNP), a self-combustion method with glycine as fuel and metal nitrates as oxidant. The stoichiometric amounts of high-purity $La(NO_3)_3{\cdot}6H_2O$, $Ni(NO_3)_2{\cdot}6H_2O$ and $Cu(NO_3)_2{\cdot}6H_2O$ were dissolved in an aqueous solution of nitric acid with subsequent addition of glycine; the glycine quantity necessary for nitrates reduction was calculated assuming $H_2O$, $CO_2$ and $N_2$ as unique gaseous reaction products. Following drying and self-combustion, the resultant powder was calcined in air at 1073 K for 2 h and subsequently mixed with LSGM powder in an agate mortar.

The system $(SrCoO_{3-\delta})_{1-x}(Sr_2Fe_3O_{6.5\pm\delta})_x$ (SCSF) was synthesized directly from the stoichiometric quantities of high-purity $Sr(NO_3)_2$, $Co(NO_3)_2{\cdot}6H_2O$ and $Fe(NO_3)_3{\cdot}9H_2O$ via the conventional synthesis route. The solid state reactions were carried out at 1273–1373 K for 10–20 h with multiple intermediate grinding steps.

The powders of all composites were uniaxilly pressed into green compacts at 250–300 MPa and then sintered in atmospheric air. The sintering conditions are listed in Table 1. Before all further studies the specimens were annealed at 1173–1273 K during 4–15 h in air and slowly cooled with furnace-controlled rate to provide oxygen stoichiometry as close as possible to equilibrium values at low temperatures.

The prepared materials have been characterized by X-ray diffraction (XRD), scanning electron microscopy coupled with energy dispersive spectroscopy (SEM/EDS), dilatometry and 4-probe DC conductivity measurements. Fullprof [27] was employed to refine structural parameters from XRD data. SEM studies were carried out by means of a Hitachi S-4100 microscope equipped with a Rontec UHV Detection system for the EDS analysis. The oxygen ionic conductivity values were estimated using measurements of steady-state oxygen

**Table 1** Abbreviations, processing conditions and thermal expansion coefficients (TECs) of oxide composite materials

| Composition | Abbreviation | Sintering conditions | | Average TECs | |
|---|---|---|---|---|---|
| | | $T$ (K) | Time (h) | $T$ (K) | $\alpha \times 10^6$ ($K^{-1}$) |
| $Ce_{0.8}Gd_{0.2}O_{2-\delta}$ | CGO | 1873 | 4 | 300–1100 | 11.5 ± 0.1 |
| $(La_{0.9}Sr_{0.1})_{0.98}Ga_{0.8}Mg_{0.2}O_{3-\delta}$ | LSGM | 1673 | 4 | 373–1273 | 11.1 ± 0.1 |
| $La_{0.8}Sr_{0.2}Fe_{0.8}Co_{0.2}O_{3-\delta}$ | LSFC | 1673 | 4 | 373–1073 | 12.9 ± 0.2 |
| $La_{0.7}Sr_{0.3}MnO_{3-\delta}$ | LSM | 1743 | 5 | 300–1100 | 11.7 ± 0.1 |
| $La_2Ni_{0.8}Cu_{0.2}O_{4\pm\delta}$ | LNC | 1503 | 2 | 400–1240 | 13.3 ± 0.1 |
| 50% (wt.) CGO/50% (wt.) LSFC | CGO/LSFC-1 | 1773 | 2 | 300–1050 | 12.6 ± 0.3 |
| | CGO/LSFC-2 | 1698–1828[a] | 12 | – | – |
| 50% (wt.) CGO/50% (wt.) LSM | CGO/LSM-1 | 1793 | 4 | 300–1100 | 11.7 ± 0.1 |
| | CGO/LSM-2 | 1793 | 2 | – | – |
| 60% (wt.) LSGM/40% (wt.) LSFC | LSGM/LSFC-1 | 1593 | 1 | 373–923 | 13.5 ± 0.1 |
| | | | | 923–1273 | 17.8 ± 0.1 |
| | LSGM/LSFC-2 | 1683 | 4 | 373–923 | 12.6 ± 0.1 |
| | | | | 923–1273 | 19.0 ± 0.1 |
| 60% (wt.) LSGM/40% (wt.) LNC | LSGM/LNC | 1503 | 2 | 373–923 | 12.9 ± 0.1 |
| | | | | 923–1273 | 15.7 ± 0.1 |
| $(SrCo)_{0.8}(Sr_2Fe_3)_{0.2}O_{3.3\pm\delta}$ | SC8SF2 | 1483 | 5 | 373–673 | 13.9 ± 0.1 |
| | | | | 673–973 | 26.3 ± 0.1 |
| | | | | 973–1193 | 33.5 ± 0.1 |
| $(SrCo)_{0.5}(Sr_2Fe_3)_{0.5}O_{4.5\pm\delta}$ | SC5SC5 | 1428 | 5 | 373–923 | 14.6 ± 0.1 |
| | | | | 923–1273 | 21.5 ± 0.1 |
| $(SrCo)_{0.2}(Sr_2Fe_3)_{0.8}O_{5.7\pm\delta}$ | SC2SF8 | 1463 | 5 | 373–923 | 13.6 ± 0.1 |
| | | | | 923–1273 | 16.8 ± 0.1 |

[a]The samples were sintered in the course of increasing temperature from 1698 to 1828 K by steps of 10–20 K. Duration of each step was 1 h

permeation fluxes. All data on oxygen permeability reported in this work corresponds to the membrane feed-side oxygen partial pressure ($p_2$) maintained at 21 kPa (atmospheric air); the permeate-side oxygen partial pressure ($p_1$) varied in the range 0.2–20 kPa. Only gas-tight samples were used for the permeation studies. Details of the equipment and experimental techniques can be found elsewhere [6, 13, 15, 19, 20, 26].

The values of the activation energy ($E_a$) for the total and oxygen ionic conductivities, presented below, were calculated by the standard Arrhenius model:

$$\sigma = \frac{A_0}{T}\exp\left(-\frac{E_a}{RT}\right) \quad (1)$$

where $A_0$ is the pre-exponential factor. For the analysis of oxygen permeation processes, the quantities permeation flux density $j$ (mol×$s^{-1}$ ×$cm^{-2}$) and specific oxygen permeability $J(O_2)$ (mol×$s^{-1}$ ×$cm^{-1}$) were used; their relationship is given by

$$J(O_2) = j.d.\left[ln\frac{p_2}{p_1}\right]^{-1} \quad (2)$$

where $d$ is the membrane thickness, $P_1$ and $P_2$ are the oxygen partial pressures at the membrane feed and permeate sides, respectively. By definition the quantity $J(O_2)$ is proportional to $j \times d$. Therefore, the specific permeability should be independent of the membrane thickness if the surface oxygen exchange limitations are negligible. In the latter case, the overall oxygen flux is determined by the bulk ambipolar conductivity ($\sigma_{amb}$) of the membrane material. The values of $\sigma_{amb}$, averaged for a given oxygen partial pressure range, were obtained from oxygen permeation flux density measurements:

$$\sigma_{amb} = \frac{16F^2d}{RT}\cdot\lim_{p_1\to p_2}\frac{\partial j}{\partial \ln(p_2/p_1)} \quad (3)$$

The oxygen ion transference number ($t_O$), partial oxygen ionic ($\sigma_O$) and electronic ($\sigma_e$) conductivities have been calculated from the total and ambipolar conductivity data using the relationship

$$\sigma_{amb} = \frac{\sigma_O\sigma_e}{\sigma_O+\sigma_e} = \frac{t_O\sigma(1-t_O)\sigma}{\sigma} = t_O(1-t_O)\sigma \quad (4)$$

where $\sigma_e$ is the sum of the n-type and p-type contributions ($\sigma_e = \sigma_n + \sigma_p$).

## Results and discussion

### CGO–LSFC system

X-ray diffraction data on CGO/LSFC ceramics (Table 2) show that these materials are dual-phase, with fluorite-type and rhombohedrally-distorted perovskite-like crystal structures, characteristic for CGO and LSFC, respectively. The perovskite unit cell in CGO/LSFC composites is smaller than in pure LSFC, while the fluorite lattice parameters refined for composites are higher than for gadolinia-doped ceria. The expansion of the ceria lattice may be associated with diffusion of lanthanum and strontium cations from the ferrite grains

**Table 2** Properties of composite ceramics and their parent materials

| Abbreviation | Space group | Unit cell parameters (Å) | | | Activation energies for total and ionic conductivities | | |
|---|---|---|---|---|---|---|---|
| | | a | b | c | Conductivity | T (K) | $E_a$ (kJ/mol) |
| CGO | Fm3m | 5.425 | – | – | Total | 723–1273 | 72.9 ± 0.8 |
| LSGM | I2/a | 7.829 | 5.546 | 5.528 | Total | 643–1223 | 96 ± 7 |
| LSFC | $R\bar{3}c$ | 5.521 | – | 13.376 | Total | 423–893 | 12.3 ± 0.5 |
| | | | | | ionic | 1073–1223 | 206 ± 9 |
| LSM | $R\bar{3}c$ | 5.503 | – | 13.351 | Total | 430–960 | 9.0 ± 0.3 |
| LNC | I4/mmm | 3.858 | – | 12.787 | Total | 320–760 | 8.6 ± 0.1 |
| | | | | | Ionic | 973–1223 | 167 ± 8 |
| CGO/LSFC-1 | Fm3m | 5.446 | – | – | total | 310–1230 | 21.5 ± 0.5 |
| | $R\bar{3}c$ | 5.505 | – | 13.337 | Ionic | 1023–1223 | 82 ± 14 |
| CGO/LSFC-2 | Fm3m | 5.451 | – | – | Total | – | – |
| | $R\bar{3}c$ | 5.508 | – | 13.344 | Ionic | 1023–1223 | 108 ± 14 |
| CGO/LSM-1 | Fm3m | 5.446 | – | – | Total | 360–1210 | 9.3 ± 0.1 |
| | $R\bar{3}c$ | 5.510 | – | 13.349 | Ionic | 1023–1223 | 106 ± 7 |
| CGO/LSM-2 | Fm3m | 5.439 | – | – | Total | – | – |
| | $R\bar{3}c$ | 5.504 | – | 13.349 | Ionic | 1023–1223 | 120 ± 9 |
| LSGM/LSFC-1 | $R\bar{3}c$ | 5.525 | – | 13.385 | Total | 298–848 | 24.0 ± 0.3 |
| | | | | | Ionic | 1073–1223 | 132 ± 9 |
| LSGM/LSFC-2 | $R\bar{3}c$ | 5.527 | – | 13.385 | Total | 298–848 | 24.9 ± 0.2 |
| | | | | | Ionic | 1023–1223 | 162 ± 7 |
| LSGM/LNC | I2/a | 7.805 | 5.527 | 5.472 | Total | 300–945 | 23.7 ± 0.4 |
| | I4/mmm | 3.854 | – | 12.748 | Ionic | 973–1223 | 122 ± 7 |
| SC8SC2 | Pm3m | 3.867 | – | – | Total | 298–730 | 23.4 ± 0.8 |
| | | | | | Ionic | 973–1173 | 146 ± 13 |
| SC5SF5 | Iba2 | 11.048 | 18.977 | 5.559 | Total | 298–808 | 39.9 ± 0.6 |
| | Pm3m | 3.868 | – | – | | 808–1296 | 20.4 ± 0.3 |
| | | | | | Ionic | 973–1173 | 138 ± 7 |
| SC2SF8 | Iba2 | 11.084 | 19.022 | 5.573 | Total | 298–630 | 34.7 ± 1.3 |
| | | | | | | 630–1314 | 15.8 ± 0.3 |
| | | | | | Ionic | 1023–1173 | 129 ± 10 |

into the fluorite phase [28]. The transition metal cations also could migrate to CGO, but their radii are lower than for rare-earth elements, and a contraction of ceria lattice should be observed in the latter case [13]. In order to confirm this hypothesis, green compacts of CGO and LSFC were pressed to each other and reacted using the sintering profile identical to CGO/LSFC-1 (Table 1). Figure 1 shows a cross-sectional view of this reaction couple. The unit cell parameter of CGO ($a_{CGO}$) increases in the vicinity of the contact area. At the opposite side of the CGO pellet the lattice constant is close to that of pure ceria. Such an expansion is indeed caused by minor incorporation of $La^{3+}$ into ceria grains as revealed by EDS analysis of LSFC and CGO in the region close to their contact (Fig. 1). Figure 2 shows EDS spectra acquired at selected CGO and LSFC regions marked as 1–4 in Fig. 1. Spectra 1 and 4 (taken far from the CGO/LSFC interface) indicate no presence of foreign cations, whilst spectra 2 and 3 (obtained close to the contact zone) suggest incorporation of Ce and, possibly, Gd into LSFC, and La into ceria. The diffusion of cerium and gadolinium cations to the LSFC grains seems rather surprisingly. The solubility of $Ce^{4+}$ ions in the lattice of perovskites, where the A-sublattice is mainly occupied by lanthanum and with transition metal cations in the B-sites, is typically low [29]. Also, the thermodynamic stability of Gd-containing perovskite-like oxides is lower than that of La-based perovskites [29, 30]. Most likely, the incorporation of cerium and gadolinium is favored by significant A-site deficiency of the perovskite phase, resulting from $La^{3+}$ and $Sr^{2+}$ diffusion into CGO grains. These phenomena could also explain the smaller fluorite unit cell parameter for CGO/LSFC-1 with respect to CGO/LSFC-2, sintered at higher temperatures and during a longer period (Table 1). Naturally, significant interdiffusion is expected for the latter composite.

The relative volume fractions of the phases have been determined using their weight ratio and theoretical densities, calculated from XRD data. For CGO/LSFC-1 ceramics, the volume ratio between CGO and LSFC is 48:52 (with accuracy of 1%), close to the expected value, and should provide percolation of both composite components. A homogeneous phase distribution was indeed illustrated by SEM micrographs of CGO/LSFC oxides (Fig. 3a and b). The grain size of CGO/LSFC-2 sintered at higher temperatures and for a longer time is 2–5 times larger than in CGO/LSFC-1.

The averaged values of the thermal expansion coefficients (TECs) were calculated from corresponding dilatometric curves. The thermal expansion of CGO/LSFC is almost linear within studied temperature range (Fig. 4). The TEC value of CGO/LSFC-1 lies between the TECs of the starting components (Table 1). For a percolated system with homogeneous microstructure the TEC of the composite results from the volume fraction and TEC of each individual phase [31].

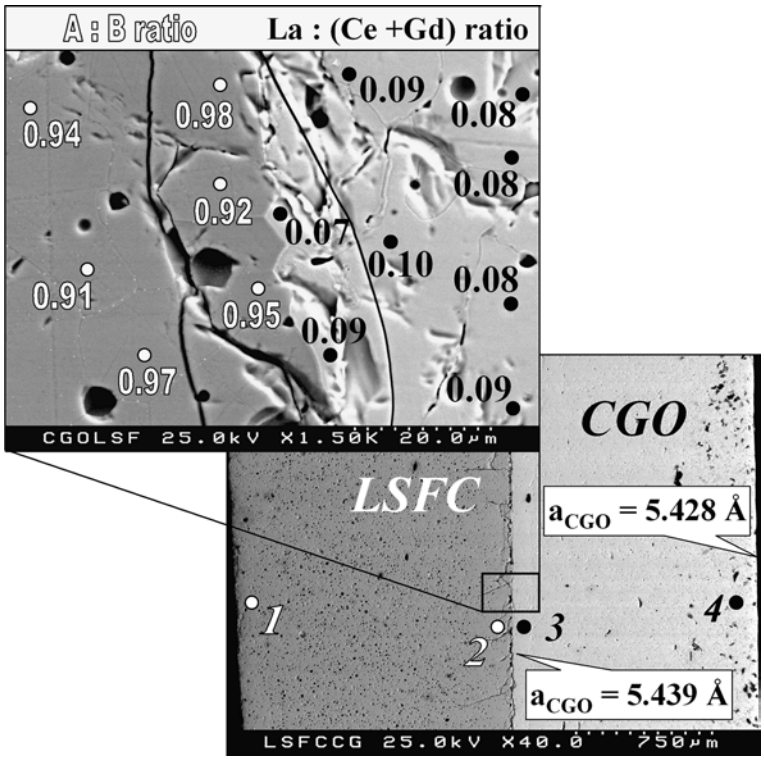


**Fig. 1** SEM micrograph of reacted CGO/LSFC couple (*bottom*) and magnified fragment of the CGO/LSFC interface (*top*). The *white* and *black numbers* in the upper micrograph show the A:B and La–(Ce + Gd) cation ratio in the corresponding points of perovskite and fluorite ceramics, respectively. *Points 1–4* in the bottom micrograph show the local areas corresponding to the EDS spectra presented in Fig. 2. The unit cell parameters ($a_{cgo}$) were calculated from the XRD data collected at the cross-sections along the direction parallel to the CGO/LSFC interphase

The total conductivity of CGO/LSFC-1, predominantly electronic, is determined by the percolated phase with the highest electrical transport (LSFC), as shown in Fig. 5. As a result, the $E_a$ values for total conductivity (Table 2) are quite similar for CGO/LSFC-1 and LSFC, whilst the $E_a$ of CGO is more than three times higher than that of the composite.

Figure 6 shows that the oxygen permeation flux level for CGO/LSFC-1 membranes is higher than for CGO/LSFC-2. Within the experimental error limits, the oxygen permeation flux through CGO/LSFC ceramics decreases with membrane thickness while the specific oxygen permeability is thickness-independent [19]. Hence, the overall oxygen ionic transport is limited by the bulk ambipolar conductivity only. The negligible influence of surface kinetics was furthermore confirmed by separate permeation tests using CGO/LSFC membranes with catalytically active porous Pt layers on both surfaces; the effect of such layers was found insignificant [19]. Due to negligible role of surface exchange kinetics, the oxygen ion transference number and oxygen ionic conductivity were calculated from the total conductivity and oxygen permeability data using Eqs. 3 and 4. $t_O$ values vary from 0.0009 to 0.0053 at 1023–1223 K, increasing with temperature. The level of ionic transport in CGO/LSFC ceramics is somewhat the average of the parent phases ionic conductivity (Fig. 7). Both, ionic conductivity and oxygen permeation flux density, in the CGO/LSFC system, decrease with increasing sintering temperature and time (Figs. 6, 7). This phenomenon results from a greater interdiffusion of the LSFC components into CGO, which decreases the solid electrolyte ionic conductivity [28]. Also, a decrease in the ionic conductivity of the perovskite phases is expected when the A-site cation radius decreases and/or vacancies are created in the A sublattice [29]. At the same time, EDS mapping of the CGO/LSFC interphase indicated the presence of substantial amount of transition cations in the solid electrolyte phase; as an example, Fig. 8 compares the cation distribution maps for gadolinium in LSFC and iron in CGO. This may increase the electronic conductivity of the ceria-based phase.

## CGO/LSM composites

The XRD studies of CGO/LSM composites detected the coexistence of two phases, one being rhombohedrally-distorted perovskite (LSM) and the other having fluorite-type crystal lattice (CGO). In a similar manner with CGO/LSFC system, the fluorite unit cell of CGO/LSM is larger than in pure CGO, whereas the perovskite lattice parameters found for composites are quite similar to those of LSFC (Table 2). The observed crystal structure expansion is more pronounced for CGO/LSM-1, prepared during a longer time than for CGO/LSM-2 (Table 1). Analogously to the CGO/LSFC, the incorporation of lanthanum cations from LSM grains into ceria might be responsible for the increasing fluorite unit cell parameter.

The volume ratio between CGO- and LSM-based phases in CGO/LSM ceramics, evaluated from XRD data, is similar to that for CGO/LSFC composites and equal to 47.7:52.3. As expected, the thermal expansion

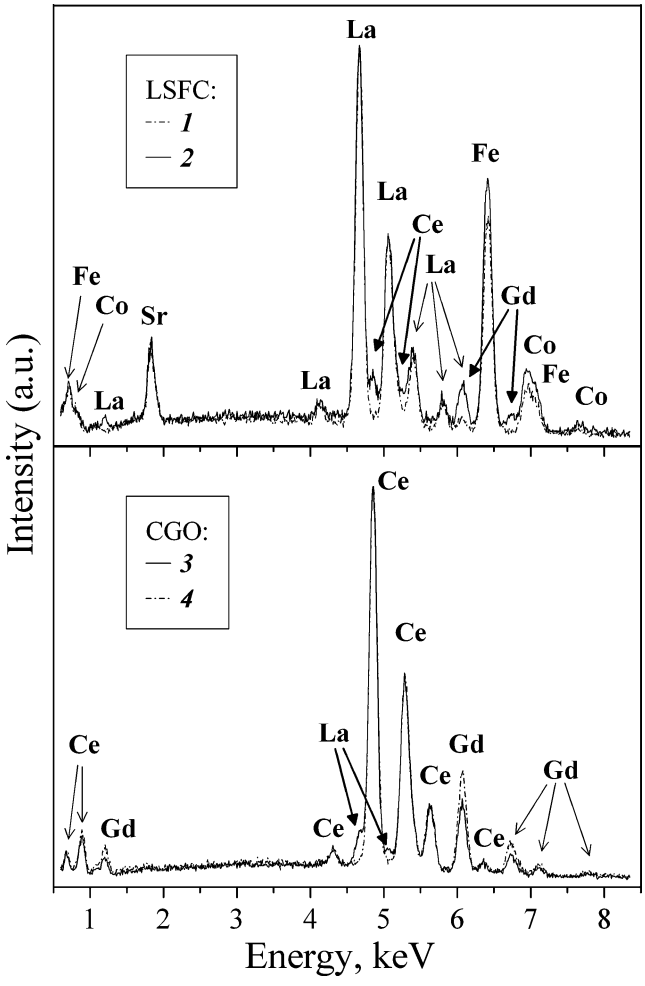


**Fig. 2** EDS spectra for the local areas of LSFC and CGO ceramics as marked in Fig. 1 (*bottom*)

of CGO/LSM-1 is linear for the studied temperatures (Fig. 9) with the average TEC value being within those of CGO and LSM (Table 1). The electrical transport in CGO/LSM oxides is predominantly electronic and its temperature dependence is similar to LSM (Fig. 5), but the values of $\sigma$ are six to eight times lower. Analogously to CGO/LSFC materials, the total conductivity in CGO/LSM ceramics is determined by the most conductive component, which is LSM in this case, and the value of $E_a$ for the CGO/LSM-1 composite coincides with that of LSM within the limits of statistical error (Table 2).

For the studied range of membrane dimensions, the oxygen permeation flux through CGO/LSM decreases with membrane thickness while the specific oxygen permeability is thickness-independent [13]. This suggests again ambipolar conductivity as permeation-limiting factor. Such a conclusion was verified by faradaic efficiency tests on the CGO/LSM materials, since the values of $t_o$ are quite similar for both techniques [13]. Estimates for $t_O$ from oxygen permeability and total conductivity data, using Eqs. 3 and 4, vary from 0.0001 to 0.0011 at 1023–1223 K, increasing with temperature. The oxygen permeation flux level and ionic conduction values are higher for CGO/LSM-2 with respect to CGO/LSM-1 (Figs. 6 and 7), sintered for a longer time. However, the ionic transport in CGO/LSM ceramics is still about ten times lower than in gadolinia-doped ceria. The interdiffusion of cations during fabrication of composites decreases the oxygen permeability and ionic conductivity of CGO/LSM materials, similarly to CGO/LSFC system.

## LSGM/LSFC ceramics

Contrary to the dual-phase systems discussed above, the LSGM/LSFC materials behave almost as single perovskite-like phases with local inhomogeneities. The perovskite structure is rhombohedrally distorted, as for LSFC (Table 2). Figure 10 illustrates that solid-state interaction between LSGM and LSFC with similar lattices is fast and takes place at low temperatures (1200–1400 K). The attempts to prepare dual-phase gas-tight samples failed, even using passivated LSGM. The perceived unit cell volume of LSGM/LSFC oxides is slightly larger than that of LSFC, but still significantly smaller than the unit cell volume of $La_{0.849}Sr_{0.139}Ga_{0.476}Fe_{0.324}Mg_{0.119}Co_{0.081}O_{3-\delta}$, the expected composition of a single perovskite phase resulting from complete reaction of LSGM and LSFC [26]. The SEM/EDS studies revealed the presence of discrete inhomogeneities visible as dark domains of ceramic grains. The amount of these regions decreases with increasing sintering temperature and time (Fig. 3c, d). According to EDS analysis, these local inhomogeneities are enriched with gallium whilst the regular ceramics body is Ga-depleted [22]. This shows a non-complete solid-state reaction between LSGM and LSFC. The interaction of the initial phases seems to occur via iron and cobalt diffusion into LSGM grains; Ga-enriched domains are kept owing to a low gallium mobility.

The dilatometric curves of LSGM/LSFC oxides show a change in slope at 900–950 K (Fig. 4). At low temperature the TEC values of LSGM/LSFC and LSFC are close to each other (Table 1). In the range 923–1273 K, the TECs increase up to 17.8–$19.0\times10^{-6}$ $K^{-1}$. Such a distinct performance of LSGM/LSFC thermal expansion in comparison with the parent phases suggests a relevant role of reaction products rather than of the original constituents, including inhomogeneous cation distribution. As for other composites, the total conductivity of LSGM/LSFC materials is mainly p-type electronic ($t_O$ increases from 0.0002 to 0.0106 when temperature increases from 1023 K to 1223 K). In spite of the almost single-phase composition, the level and $E_a$ for electrical transport in LSGM/LSFC coincide with those of dual-component CGO/LSFC-1 (Fig. 5 and Table 2). This phenomenon would not be surprising if both the rhombohedrally- and monoclinically-distorted perovskites (LSFC and LSGM, respectively) were kept in LSGM/LSFC oxides.

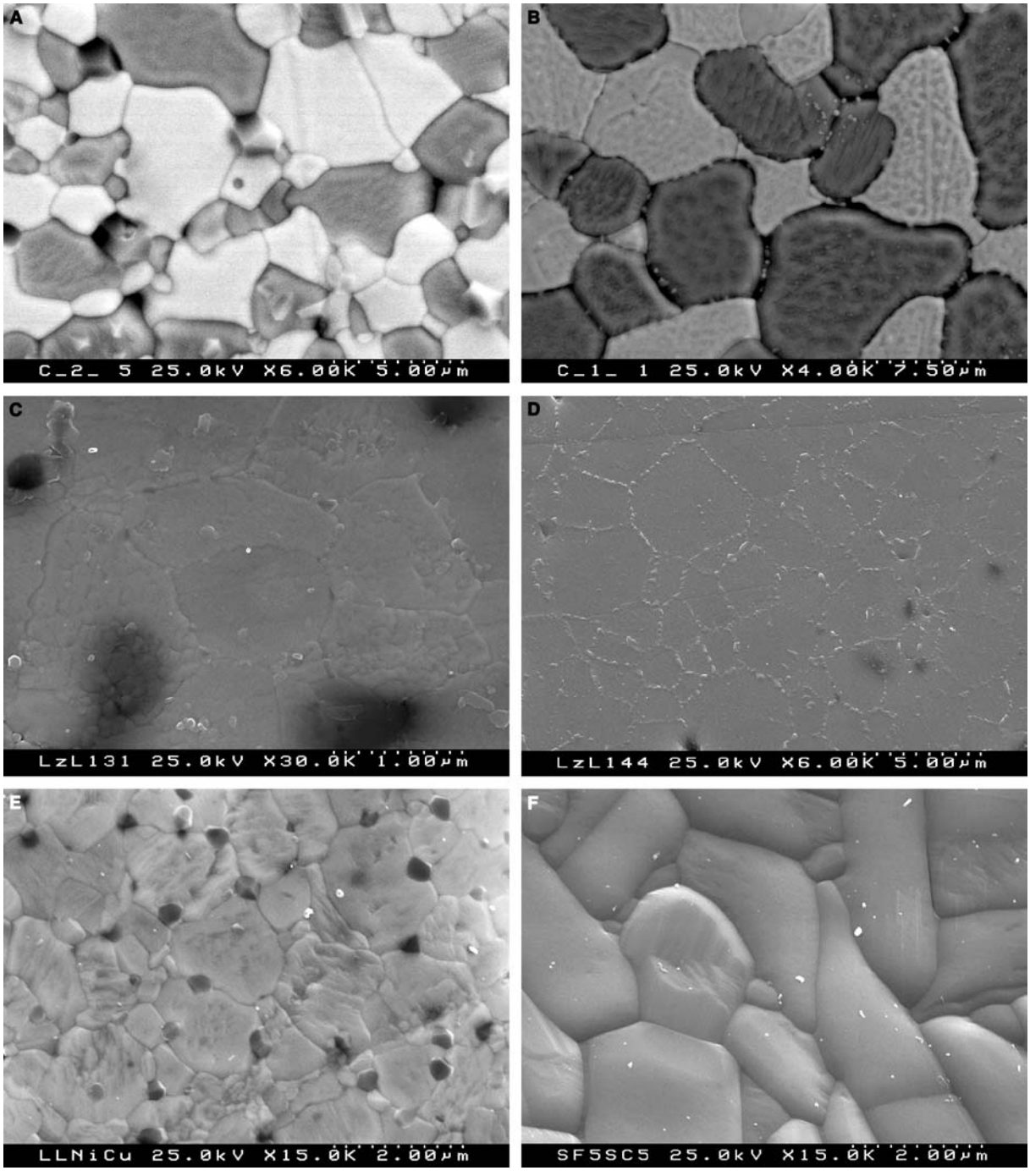


**Fig. 3** SEM micrographs of composite ceramics: CGO/LSFC-1 **a**, CGO/LSFC-2 **b**, LSGM/LSFC-1 **c**, LSGM/LSFC-2 **d**, LSGM/LNC **e** and SC5SF5 **f**

The overall oxygen conduction in LSGM/LSFC ceramics is limited by both the bulk ambipolar conductivity and surface processes, since the specific oxygen permeability values increase and permeation flux decreases with membrane thickness [22]. The maximum oxygen permeation was found for LSGM/LSFC-1 sintered at minimum temperature and time. This material exhibits higher performance with respect to CGO/LSM and CGO/LSFC (Fig. 6), although the $t_O$ and $\sigma_O$, calculated from permeability results and total conductivity data, are lower than the true, surface-unaffected values due to considerable gas–solid exchange limitations. The apparent ionic conductivity of LSGM/LSFC-1 at 1073–1223 K is two to five times lower than that of LSGM (Fig. 7). The ionic transport in LSGM/LSFC-2 is significantly lower in comparison with LSGM/LSFC-1 (Figs. 6, 7) assuming a negative effect of the interdiffusion of iron, cobalt and gallium

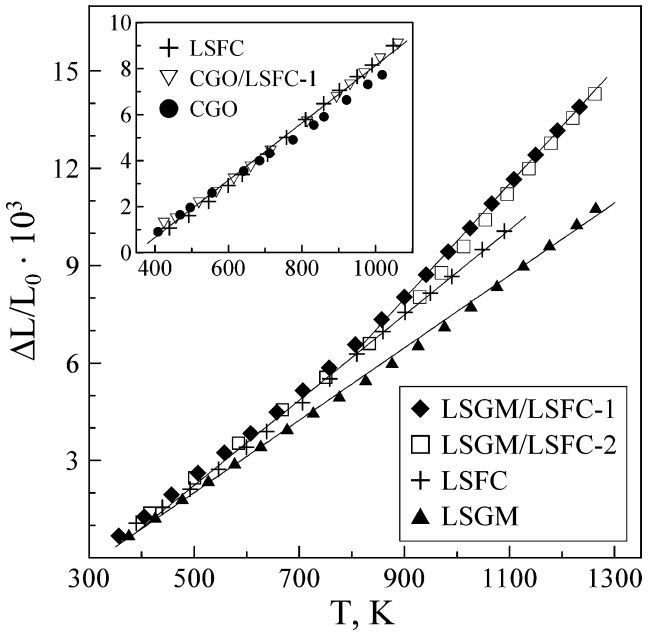


**Fig. 4** Dilatometric curves of LSGM/LSFC-1, LSGM/LSFC-2, LSFC and LSGM ceramics in air. The *inset* shows the thermal expansion of CGO/LSFC-1, CGO and LSFC

cations on the transport properties in LSGM/LSFC system.

## LSGM/LNC composites

The fast interdiffusion observed between LSGM and LSFC with similar crystal structure and comparable unit

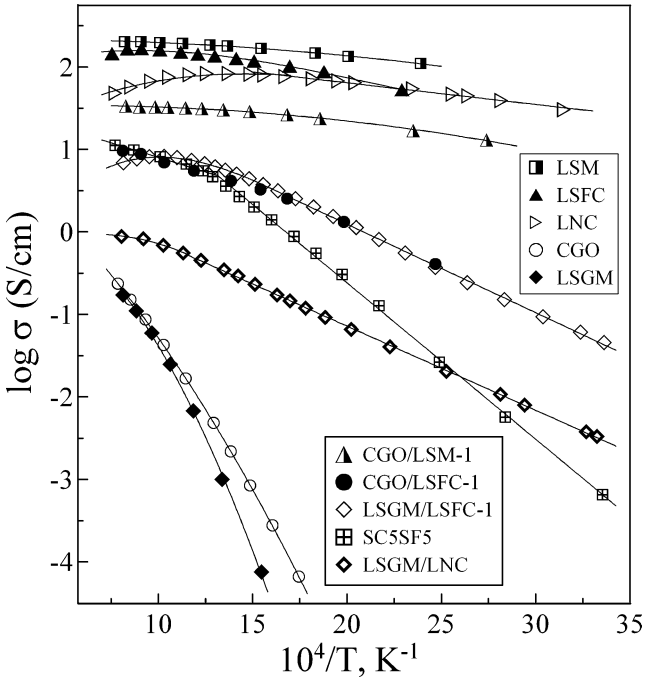


**Fig. 5** Temperature dependence of total conductivity of the composite ceramics and their parent materials, in air

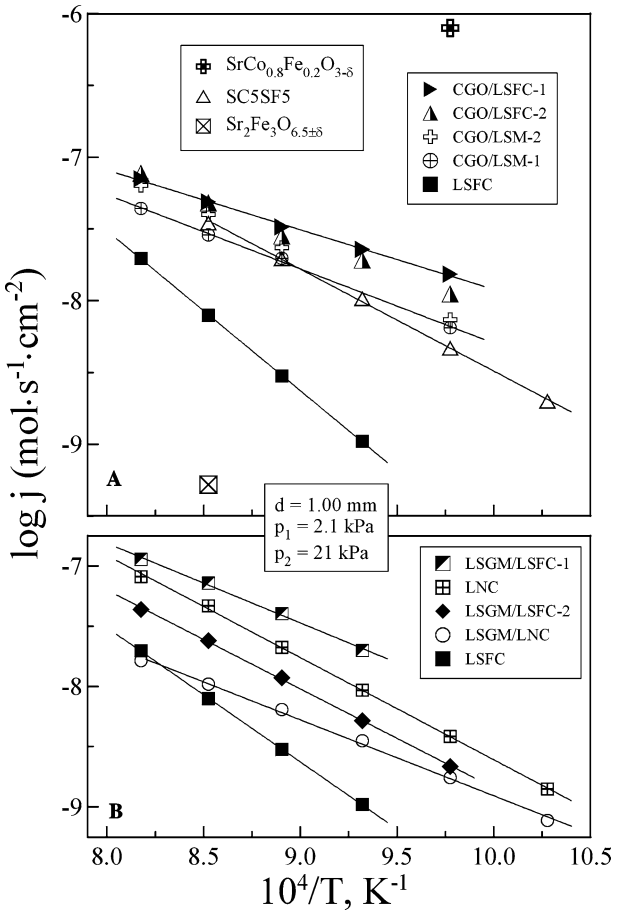


**Fig. 6** Temperature dependence of the oxygen permeation fluxes through composite membranes under fixed oxygen pressure gradient

cell volume (resulting in apparent single phase formation), suggested that the electronically-conducting component should be changed in order to try to obtain dual-phase materials with LSGM as electrolyte. For this purpose, the mixed conductor $La_2Ni_{0.8}Cu_{0.2}O_{4\pm\delta}$ having $K_2NiF_4$-type structure was synthesized. This phase consists of alternating perovskite and rock-salt type layers. Contrary to LSGM/LSFC system, no continuous solid solution via interaction of LSGM and LNC is expected. The dilatometric tests of LSGM/LNC green compacts revealed their shrinkage being even more extensive than in the case of LSGM/LSFC materials, although occurring at higher temperatures (Fig. 10). Such a behavior is typical for reacting systems. The XRD analysis of LSGM/LNC ceramics indeed detected about 4.9%vol. of Roddlesden–Popper type $La_2Ni_3O_7$-based impurity (Fig. 11), in addition to LSGM (69.1%vol.) and LNC (26.0%vol.), while the volume ratio between LSGM and LNC should be 61.2:38.8 assuming non-reacting starting phases. The microstructure of LSGM/LNC oxides is inhomogeneous and consists of larger grains of the parent components and smaller grains (dark in SEM micrographs) of the segregated phase (Fig. 3e). The EDS studies revealed that

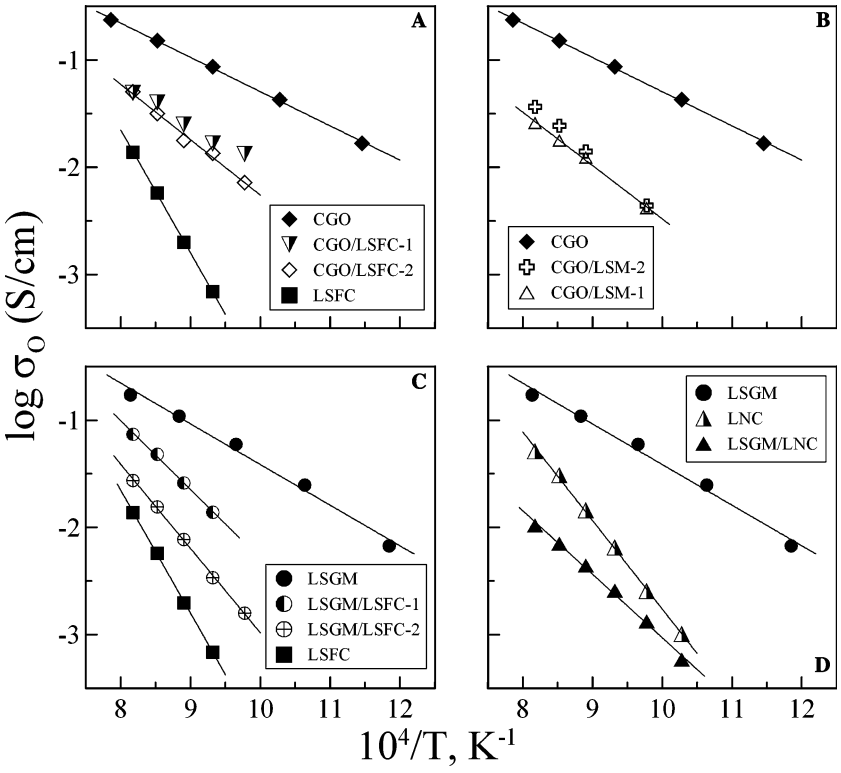


**Fig. 7** Temperature dependence of the oxygen ionic conductivity of composite materials in air

the latter spots are enriched with magnesium and nickel, in comparison with the larger grains (Fig. 12). In combination with XRD data this fact discloses $La_3(Ni,Mg)_3O_7$ solid solution formation and magnesium depletion of LSGM, that may affect the transport properties of LSGM/LNC.

The values of relative thermal expansion of LSGM/LNC and LNC are sufficiently close, though the dilatometric dependence of LSGM/LNC undergoes a break nearby 900–950 K (Fig. 9). At 373–923 K the average TEC of the composite is between those of parent oxides and becomes higher than for LNC on further heating (Table 1). The $E_a$ of total conductivity in LSGM/LNC is similar to LSGM/LSFC and CGO/LSFC (Table 2), but the level of electrical transport is about ten times lower (Fig. 5), showing a loss in percolation of LNC grains, in agreement with a quite low LNC content to values, increasing with temperature, vary in the range

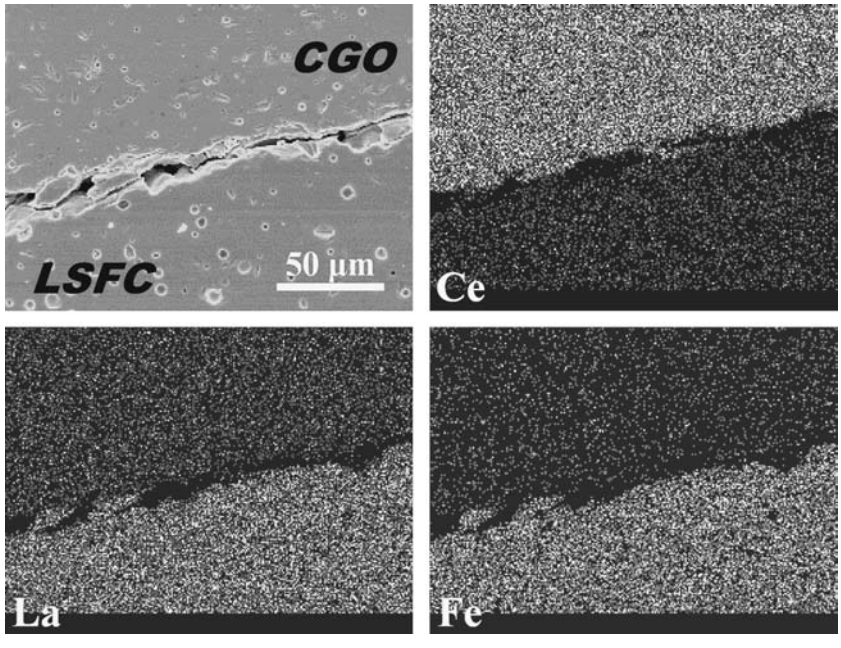


**Fig. 8** Cation distribution maps near CGO/LSFC interface

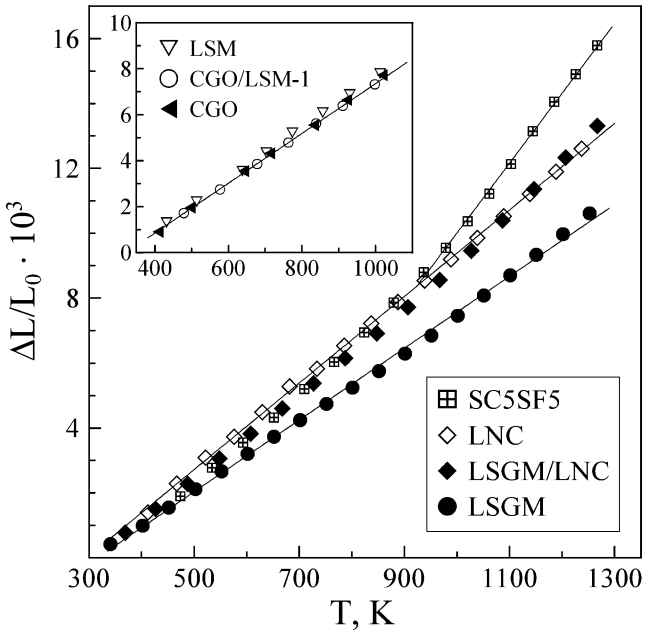


**Fig. 9** Dilatometric curves of LSGM/LNC, LSGM, LNC and SC5SF5 ceramics in air. The *inset* shows the thermal expansion of CGO/LSM-1, CGO and LSM

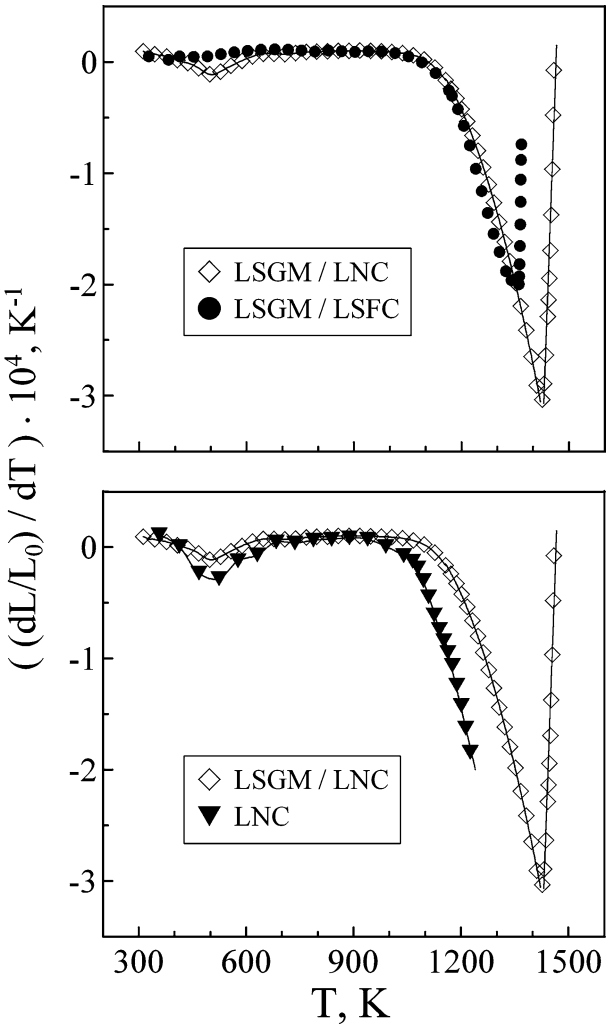


**Fig. 10** Differential shrinkage curves for LSGM/LSFC, LSGM/LNC and LNC green compacts

0.0009–0.0118 at 973–1223 K. Hence, the electronic conduction in LSGM/LNC is dominant regardless the high volume fraction of the solid electrolyte. Likely, the contacting layers of electronically conducting phases separate LSGM grains, suppressing the ionic transport. The oxygen specific permeability of LSGM/LNC is thickness-independent while permeation fluxes decrease with membrane thickness (Fig. 13). This indicates insignificant influence of oxygen surface exchange rate on the overall process. Both the permeation flux density and ionic conductivity of LSGM/LNC are lower than those of LNC being the lowest among the composites presented in this work (Figs. 6, 7). LSGM and LNC lead to additional phase formation, and the transport characteristics of the resulting material are poor.

### $SrCoO_{3-\delta}$ – $Sr_2Fe_3O_{6.5\pm\delta}$ system

The SCSF ceramics having little Fe are cubic perovskites with cobalt oxide impurities (Fig. 11). Cobalt cations in $SrCoO_{3-\delta}$ are replaced by iron and $Sr_2Fe_3O_{6.5\pm\delta}$ is not formed. Another extreme composition of this series, SC2SF8, has the orthorhombic $Sr_2(Fe,Co)_3O_{6.5\pm\delta}$-type crystal lattice and is single-phase (Table 2). In the latter structure perovskite-like sheets of corner-sharing $FeO_6$ octahedra are alternated with $(Fe,Co)O_4$ and $(Fe,Co)O_5$ polyhedra layers; the incorporation of strontium excess is compensated, most likely, by vacancies in the iron and oxygen sublattices. The dual-phase material has been obtained in the case of the SC5SF5 composite (Fig. 11). The volume ratio between the perovskite- and $Sr_2(Fe,Co)_3O_{6.5\pm\delta}$-type phases is 20:80, considerably lower than the value calculated using $(SrCo)_{0.5}(Sr_2Fe_3)_{0.5}O_{4.5\pm\delta}$ as nominal composition (28.4:71.6). The phase composition of both the SC5SF5 and SC2SF8 indicates that $Sr_2(Fe,Co)_3O_{6.5\pm\delta}$-like structure may tolerate some Fe-site deficiency. The average grain size of two-phase SC5SF5 varies from 1 μm to 2 μm (Fig. 3f). The dilatometric curve of SC5SF5 shows a change in line slope at 900–950 K (Fig. 9). Although the presence of the layered phase decreases the thermal expansion, the average TECs are still high, in the range 13.8–$14.6\times10^{-6}$ $K^{-1}$ at low temperatures and 17.1–$28.1\times10^{-6}$ $K^{-1}$ above 700–900 K (Table 1). The total conductivity of SC5SF5 at 800–1300 K is close to the level of electrical transport in CGO/LSFC-1 and LSGM/LSFC-1 (Fig. 5). At lower temperatures the $E_a$ of the total conduction increases and $\sigma$ values change significantly faster. The ionic conductivity $E_a$ values are essentially independent of composition (Table 2). The level of permeation flux density for SC5SF5 composite is comparable with CGO/LSM membranes (Fig. 6).

Although fabrication of dual-phase composites consisting of $Sr_4Fe_6O_{13}$ - and perovskite-type solid solutions

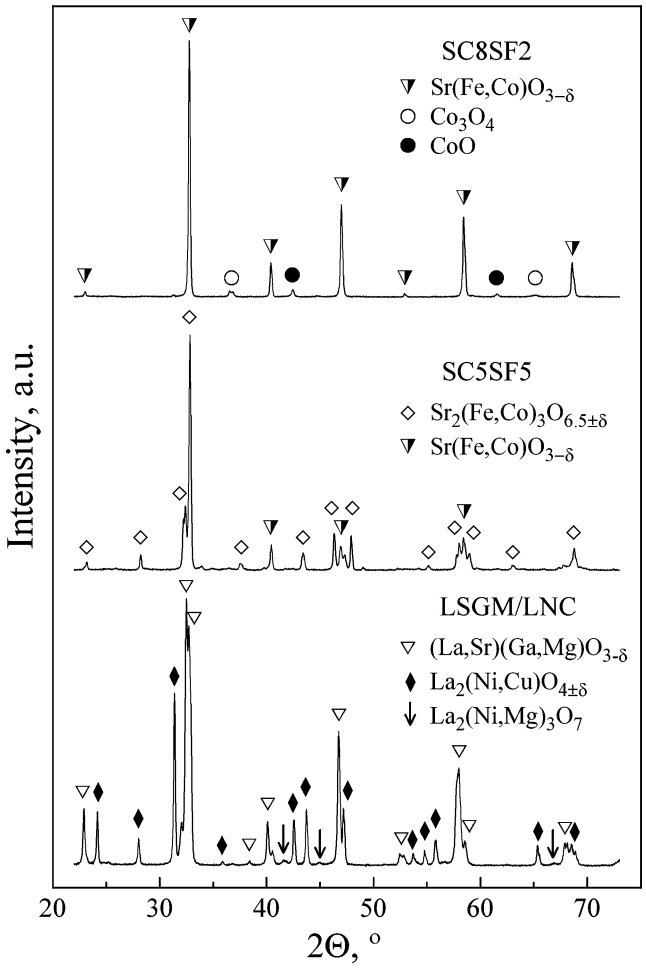


**Fig. 11** XRD patterns of SC8SF2, SC5SF5 and LSGM/LNC ceramics

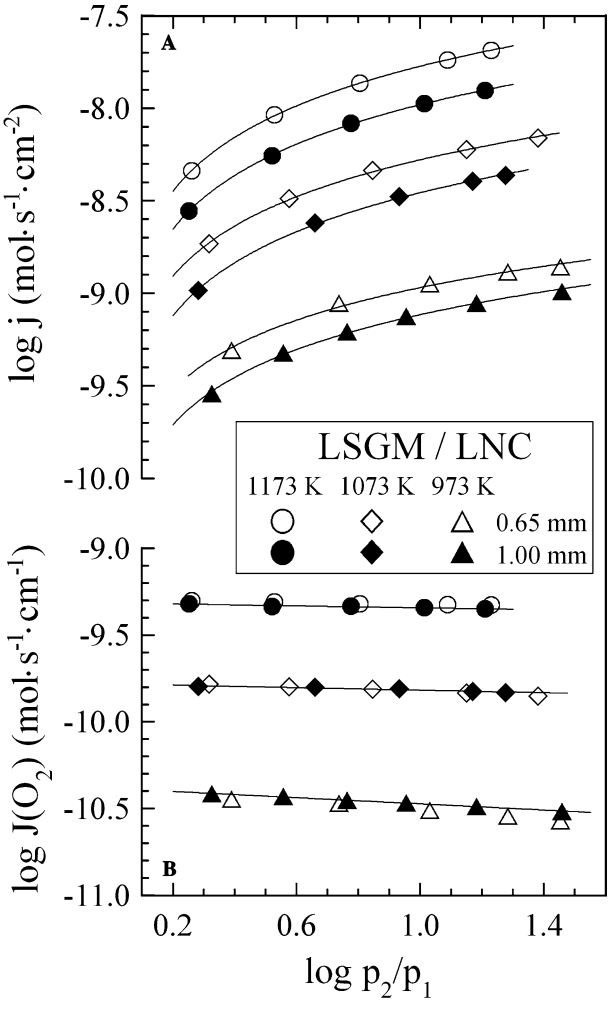


**Fig. 13** Oxygen permeation flux **a** and specific oxygen permeability **b** of LSGM/LNC membranes with various thickness

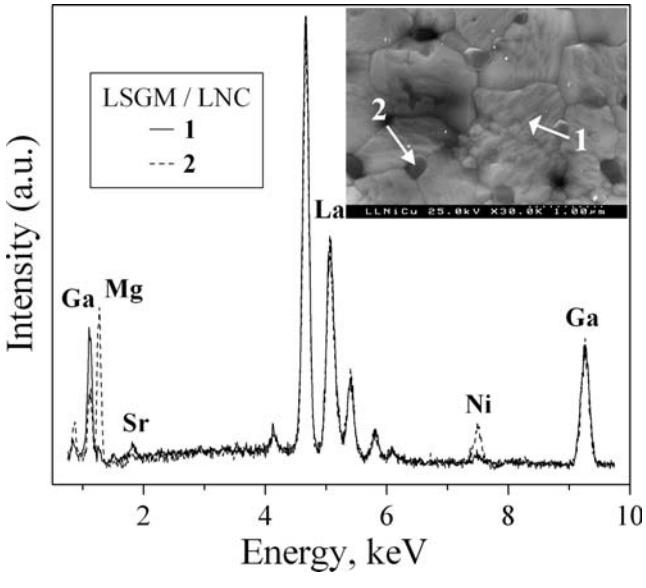


**Fig. 12** EDS spectra of LSGM/LNC composite grains marked in the SEM micrograph (*inset*)

is possible at comparable concentrations of iron and cobalt, this combination of phases cannot provide a significant improvement of the membrane properties, again due reaction between phase constituents. The thermal expansion of SCSF series composites is excessive, as for $Sr(Co,Fe)O_{3-\delta}$ perovskites, whilst the oxygen permeability is significantly lower if compared to the latter compounds.

## Final remarks

Traditional ceramic routes are still the most obvious alternative to prepare composites with preservation of the characteristics of the individual constituents, preventing extensive reaction, formation of new phases and blocking interfaces, etc. Chemical routes, with intimate mixing of all cations at some early stage of preparation, are unlikely to be of any use for the present purpose. In fact, they enhance materials interaction. The same applies to interesting but hardly effective solutions like solidification from melts. Although well known from the

literature, adoption of all such alternative routes for composites processing was though as useless in the present cases.

For conventional ceramic routes, ideal conditions are obtained from a compromise between starting powder characteristics and firing conditions, in order to ensure the effectiveness of sintering and related mass transport processes, but preventing extensive interaction between constituents, to avoid significant compositional changes. Ideal conditions are hardly met in practice, and the result is obviously determined by the kinetic parameters determining the diffusion and/or formation of new phases from the initial constituents, for a given set of firing conditions.

Inert starting materials would be ideal for the present purpose. Noble metals and some fluorite based solid electrolytes are the closest examples to this condition, but their use is by no means acceptable from an economic perspective, and their performance is somewhat limited [9, 10, 14]. This lengthy series of remarks was needed to explain the constraints faced in the present case. These remarks are also needed to emphasize that the present work is by no means exhaustive. Exploitation of other experimental conditions might provide better results, but this is a never ending process.

Moving again to the exploited systems, we can easily recognize that the best microstructural results were obtained with the CGO based composites. This is obviously due to the poor solubility and/or reactivity of ceria with respect to the remaining constituents (LSM and LSCF). Although this result was the closest to the ideal "composite approach" adopted in the present work, the best performance was observed for the LSGM/LSCF combination, where interaction between the starting materials was so high that almost complete reaction could be observed, with formation of a new phase with only local inhomogeneities. This result suggests a careful analysis of the performance of complex perovskites, with multiple cations in both lattice positions (mostly in the B-site, as the La,Sr combination for the A-site is almost a standard). Furthermore, this also opens a new potential direction for research on materials with local inhomogeneities within the grain size scale, suggesting that such materials, with internal compositional gradients, might perform better than composites.

## Conclusions

The electrical conductivity, thermal expansion and ionic transport in composite ceramics $Ce_{0.8}Gd_{0.2}O_{2-\delta}$ – $La_{0.8}Sr_{0.2}Fe_{0.8}Co_{0.2}O_{3-\delta}$, $Ce_{0.8}Gd_{0.2}O_{2-\delta}$ – $La_{0.7}Sr_{0.3}MnO_{3-\delta}$, $(La_{0.9}Sr_{0.1})_{0.98}Ga_{0.8}Mg_{0.2}O_{3-\delta}$ – $La_{0.8}Sr_{0.2}Fe_{0.8}Co_{0.2}O_{3-\delta}$, $(La_{0.9}Sr_{0.1})_{0.98}Ga_{0.8}Mg_{0.2}O_{3-\delta}$ – $La_2Ni_{0.8}Cu_{0.2}O_{4+\delta}$, and $SrCoO_{3-\delta}$ – $Sr_2Fe_3O_{6.5\pm\delta}$ were studied. In most cases, the interdiffusion of cations between the phases does not affect considerably the electronic conductivity, while the ionic transport was found to decrease with increasing interaction between components. The level of interaction is much lower for the compositions where no solid solutions or reaction is observed. Similar crystal structures of starting oxides may result in almost single-phase ceramics with local inhomogeineties, but still high permeation. The formation of Roddlesden–Popper phase in LSGM/LNC has a deteriorating effect on the transport characteristics of the final material. The role of components reactivity may become critical under operation conditions when the cation interdiffusion is significant, thus leading to a time degradation in the performance of electrochemical devices, such as oxygen membranes and solid oxide fuel cells.

**Acknowledgements** This work was supported by the FCT, Portugal (POCTI program and projects BD/6595/2001 and BPD/15003/2004), and the NATO Science for Peace program (project 978002). Experimental assistance and helpful discussions, made by E. Tsipis, F. Figueiredo and N. Vyshatko, are gratefully acknowledged.

## References

1. Bouwmeester HJM, Burggraaf AJ (1996) Fundametals of inorganic membrane science and technology. Elsevier, Amsterdam, pp 435–528
2. Porat O, Heremans C, Tuller HL (1997) Solid State Ionics 94:75
3. McEvoy AJ (2000) Solid State Ionics 132:159
4. Wilhelm DJ, Simbeck DR, Karp AD, Dickenson RL (2001) Fuel Process Technol 71:139
5. Mazanec TJ, Prasad R, Odegard R, Steyn C, Robinson ET (2001) Stud Surf Sci Catal 136:147
6. Kharton VV, Yaremchenko AA, Kovalevsky AV,Viskup AP,Naumovich EN, Kerko PF (1999) J Membr Sci 163:307
7. Mazanec TJ (1997) Ceramic Membranes I, PV 95–24. The Electrochemical Society, Pennington, pp 16–28
8. Shen Y, Joshi A, Liu M, Krist K (1994) Solid State Ionics 72:209
9. Chen CS, Boukamp BA, Bouwmeester HJM, Cao GZ, Kruidhof H, Winnubst AJA, Burggraaf AJ (1995) Solid State Ionics 76:23
10. ten Elshof JE, Nguyen NQ, den Otter MW, Bouwmeester HJM (1997) J Electrochem Soc 144:4361
11. Chen CS, Burggraaf AJ (1999) J Appl Electrochem 29:355
12. Park YM, Choi GM (1999) J Electrochem Soc 146:883
13. Kharton VV, Kovalevsky AV, Viskup AP, Figueiredo FM, Yaremchenko AA, Naumovich EN, Marques FMB (2000) J Electrochem Soc 147:2814
14. Kim J, Lin YS (2000) J Membr Sci 167:123
15. Kharton VV, Kovalevsky AV, Viskup AP, Figueiredo FM, Yaremchenko AA, Naumovich EN, Marques FMB (2001) J Eur Ceram Soc 21:1763
16. Wu K, Xie S, Jiang GS, Liu W, Chen CS (2001) J Membr Sci 188:189
17. Nigge U, Wiemhofer H-D, Romer EWJ, Bouwmeester HJM, Schulte TR (2002) Solid State Ionics 146:163
18. Wang H, Yang WS, Cong Y, Zhu X and Lin YS (2003) J Membr Sci 224:107
19. Kharton VV, Kovalevsky AV, Viskup AP, Shaula AL, Figueiredo FM, Naumovich EN, Marques FMB (2003) Solid State Ionics 160:247
20. Kharton VV, Tsipis EV, Yaremchenko AA, Frade JR (2004) Solid State Ionics 166:327
21. Teraoka Y, Nobunaga T, Okamoto K, Miuara N, Yamazoe N (1991) Solid State Ionics 48:207

22. Pei S, Kleefisch MS, Kobylinsky TP, Faber J, Udovich CA, Zhang-McCoy V, Dabrowski BD, Balachandran U, Mieville RL, Poeppel RB (1995) Catal Lett 30:201
23. Maiya PS, Balachandran U, Dusek JT, Mieville RL, Kleefisch MS, Udovich CA (1997) Solid State Ionics 99:1
24. Fossdal A, Sagdahl LT, Einarsud M-A, Wiik K, Grande T, Larsen PH, Poulsen FW (2001) Solid State Ionics 143:367
25. Manthiram A, Prado F, Armstrong T (2002) Solid State Ionics 152–153:647
26. Shaula AL, Kharton VV and Marques FMB (2004) J Eur Ceram Soc 24:2631
27. Rodriguez-Carvajal J (1993) Physica B 192:55
28. Inaba H, Tagawa H (19996) Solid State Ionics 83:1
29. Kharton VV, Yaremchenko AA, Naumovich EN (1999) Solid State Electrochem 3:303
30. Yokokawa H, Sakai N, Kawada T, Dokiya M (1992) Solid State Ionics 52:43
31. Figueiredo FM, Marques FMB, Frade JR (2001) Solid State Ionics 138:173